PCCP

Accepted Manuscript

ROYAL SOCIETY OF CHEMISTRY

www.rsc.org/pccp

CO oxidation mechanism on W(111) surface and W helical nanowire by the density functional theory calculation

Ken-Huang Lin[1], Shin-Pon Ju[1,2,*], Jia-Yun Li[1], and Hsin-Tsung Chen[3]

[1]*Department of Mechanical and Electro-Mechanical Engineering, National Sun Yat-Sen University, Kaohsiung 804, Taiwan*

[2] *Department of Medicinal and Applied Chemistry, Kaohsiung Medical University, Kaohsiung 807, Taiwan*

[3] *Department of Chemistry, Chung Yuan Christian University, Chungli District, Taoyuan City 32023, Taiwan*

Abstract

Two CO oxidation reactions ($CO + O_2 \rightarrow CO_2 + O$ and $CO + O \rightarrow CO_2$) were considered in the Eley-Rideal (ER) reaction mechanism. These oxidation processes on the W(111) surface and W helical nanowire were investigated by the density functional theory (DFT) calculation. The stable adsorption sites of O_2 and O as well as their adsorption energies were obtained first. In order to understand the catalytic properties of W helical nanowire, the Fukui function and local density of state (LDOS) profiles were determined. The nudged elastic band (NEB) method was applied to locate transition states and minimum energy pathways (MEPs) of CO oxidation processes on the W helical nanowire and on the W(111) surface. In this study, we have demonstrated that the catalytic ability of W helical nanowire is superior to that of W(111) surface for the CO oxidation.

Keywords: W(111) surface, W helical nanowire, the density functional theory, local density of state, minimum energy pathway.

Introduction

According to the past studies, it has been found that tungsten (W) and W-based metals possess good catalytic activities for some specific gas molecules, such as CO_x [1], H_2S [2], and NO_x [3]. For example, W carbides have been used as electrocatalysts, co-catalysts, catalyst supports, and electrolytes in different types of fuel cells. WC and W_2C are also demonstrated to possess a Pt-like characteristic in a variety of catalytic reactions [4]. Many previous studies have reported the interaction mechanisms of O [5-10], O_2 [11], CO [1, 12], and CO_2 [1] on the W single crystal surfaces. These studies can partially provide some useful information about the mechanism steps for the CO oxidation reaction including the adsorptions of reactants, dissociation of O_2, and desorption of CO_2.

The W(111) surface is more structurally open than the close-packed surfaces of W(100) and W(110). Therefore, the W(111) surface can accommodate more adsorbates per unit surface and has a much higher sticking probability. Chen *et al.* [12] explored the adsorption and dissociation mechanisms of the CO molecule on the W(111) surface by the DFT calculation. They found the activation energy of CO dissociation is about 0.8 eV, which is smaller than the barrier of a CO molecule desorbed from the surface. By the DFT calculation, the adsorption and dissociation mechanisms of CO and CO_2 on W(111) surface were investigated in Chen's study [1]. The molecular structures, vibration frequencies, and binding energies of W(111)/CO_2, W(111)/CO, W(111)/C, and W(111)/O systems were reported. From the results of these studies, O_2 adsorbed on a top (T) site (located at the top of a W atom) with the side-on configuration is the most stable configuration, whereas the O atom prefers to adsorb on the bridge site (located between two four-coordinated W atoms). In addition, the CO molecule also prefers to coordinate to a bridge site with the lying-down coordination where the C and O atoms are bound preferentially on the

bridge and top sites of metal surface, respectively.

In our previous study [13], we have investigated the CO oxidation processes in the Eley−Rideal (ER) and Langmuir−Hinshelwood (LH) mechanisms on the W(111) surface and W_{10} nanoparticle. The two reaction barriers (0.16 and 0.62 eV) of pathway ($O_{2(ads)} + CO_{(gas)} \rightarrow O_{(ads)} + O_{(ads)} + CO_{(gas)} \rightarrow CO_{2(gas)}$) for the W_{10} surface are lower than the barrier (0.92 eV) for the W(111) surface, indicating that the formation of CO_2 on the W_{10} surface occurs more easily than that on the W(111) surface. These results demonstrate that the shape and size effects of nano-materials have the strong influences on the catalytic activities and electronic properties of catalysts [14, 15]. For the one-dimension transition metal materials, An *et al.* [16] investigated the oxidation properties of CO molecule on the single-walled helical Au(5,3) nanowire by the DFT calculation. They found that the CO and O_2 were co-adsorbed on the Au(5,3) helical nanowire, and formed the peroxo-type (OOCO) in the exothermic process; it only needs to pass through a very small barrier. This result represents that the nanowire exactly possesses the high activity for the CO oxidation.

To understand the catalytic ability of one-dimension nanomaterial, the W nanowire was chosen to be the basic material for investigating CO oxidation mechanism and to compare with W(111) surface. The W nanowire structure with the lowest energy was constructed by the simulated annealing basin-hopping (SABH) method and the DFT calculation was further used to study the structural and adsorption properties of CO and O_2 on the W nanowire and on the W(111) surface. Furthermore, the reaction barriers and electronic properties in the CO oxidation processes were also investigated in this work. According to all reaction barriers for the CO oxidation mechanisms on the W_{10} surface and on the W(111) surface in our previous study [13], it can be seen both the W_{10} nanoparticle and W(111) surfaces prefer the ER mechanism. Consequently, only the ER mechanism was considered in the current study and the

co-adsorption of CO_2 and O_2 for LH mechanism was not discussed. We believe this study is vital for understanding the factors affecting the CO oxidation catalyzed by the nanometer-scale tungsten nanowire.

Simulation model

All DFT calculations were employed by the DMol^3 package with the spin polarization [17]. To investigate the adsorption properties of molecules on the metal surface, the generalized gradient approximation (GGA) with the revised Perdew−Burke−Ernzerhof (rPBE) [18] density functional was used. The calculations were carried out by using the (1 × 1 × 6) and (3 × 4 × 1) Monkhorst−Pack mesh k-points for the W helical nanowire and W(111) surface, respectively. For all calculations, the convergences of total energies for the electronic step and the ionic step were set as 1×10^{-5} Ha and 2×10^{-5} Ha, respectively.

The structure of W helical nanowire is shown in Figure 1(a). This structure possesses the global mimimal energy among all structures by the SABH method search [19] with the tight-binding (TB) potential [20]. The detailed global minimal search procedure for the W nanowire can be found in our previous study [21]. The structure from the SABH was then optimized by the DFT calculation, and the optimized structure has the length of 27.9 Å along the periodic axial direction. In the configuration of W helical nanowire, four one-atom chains entangle with a helical angle of 12.07° to form a helical structure, which is designated as the helical nanowire. The helical nanowire is quite similar to the structure found in the previous study by using a TB potential through the genetic algorithm search [22].

For the W(111) surface, the calculations for the CO adsorption on $p(3 \times 2)$ and $p(3 \times 3)$ lateral cells of the W(111) surface were conducted, which correspond to the

coverage of 1/6 ML and 1/9 ML. These studies show that the coverage effect on the calculated stability of this species is negligible (smaller than 0.1 eV). Therefore, the computationally less expensive $p(3 \times 2)$ W(111) surface was used as the simulation model. The $p(3 \times 2)$ lateral cell of W(111) surface was modeled as the periodically repeated slab with 6 layers, as shown in the right panel of Figure 2. The bottom three atomic layers were kept frozen and set to the experimentally estimated bulk parameters, and the remaining layers were fully relaxed during the calculations. The lateral cell has dimensions of a = 13.5 Å, b = 7.80 Å, and c = 17.47 Å including a vacuum region of thickness 15 Å upon the W(111) substrate, which guarantees no interactions between the upper and lower slabs of the W(111) substrate.

In this study, the adsorption energies were calculated according to the following equation:

$$\Delta E_{ads} = E[\text{total}] - (E[\text{substrate}] + E[\text{CO}] + E[\text{O}_2(\text{or O})]) \quad (1)$$

In the aforementioned equation, the E[total], E[substrate], E[CO], and E[O_2(or O)] correspond to the electronic energies of adsorbed species on the W substrate, the bare W substrate, gaseous CO, and gaseous O_2 (or O), respectively. Here E is the electronic energy calculated at 0 K in vacuum. Therefore, the negative adsorption energy indicates a stable adsorption state.

The nudged elastic band (NEB) method [23, 24] was applied to locate the transition states and the corresponding minimum energy pathways (MEPs). The NEB method is an efficient method for finding the minimum energy pathway between the given initial and final states of a transition state. Sixteen images were used to locate each transition state (TS) for the NEB method.

Results and discussion

To make certain that our DFT approach is appropriate for the tungsten material,

Table 1 lists the calculated lattice constant and the cohesive energy compared with experimental values of tungsten body center cubic (BCC), face centered cubic (FCC), and hexagonal close packed (HCP) lattices [25, 26]. The cohesive energies of different tungsten configurations are close to the bulk values in experiments. Moreover, the lattice constant is 3.16 Å in BCC, which is also in agreement with the experimental values of 3.16 Å and 3.25 Å [26, 27]. The functional, basis set, and core treatment of rPBE, DND, and DSPP were employed to calculate the bond length, vibration frequency, and dissociation energy of tungsten dimer and the calculation results are listed in Table 2. Comparing with previous experimental and theoretical studies, the bond length of dimer is 2.075 Å, and the frequency and dissociation energy are 334.2 cm^{-1} and 4.74 eV, which are very close to the experimental values [28, 29]. These results represent the setups of rPBE/DND/DSPP are reasonable in this work. In the calculations of adsorbents, the bond distances of gas phase O_2, CO and CO_2 were also predicted to be 1.232 Å (O–O for O_2), 1.147 Å (C–O for CO) and 1.177 Å (C–O for CO_2) in a 15×15×15 $Å^3$ cubic box, which are also in good agreement with available experimental data and theoretical results (1.21 Å for O–O of O_2 [30]; 1.15 Å for C–O of CO [31]; 1.16 Å for C–O of CO_2 [31]).

It is difficult to recognize and determine the regions of activation directly for the helical W nanowire, because the possible adsorption sites of helical W nanowire are not simply symmetrical as those of perfect crystal surfaces. In our previous study for finding the most reactive adsorption site of a W_{10} nanocluster [13], three possible criterions including the orbital roughness [31], Fukui function [32], and the coordination number [33] were used. The Fukui function was found to be the best criterion for finding the most reactive adsorption sites for CO oxidation process. In this study, Fukui indices were computed for describing the electronic distribution.

Parr *et al.* stated the atom with the largest value of Fukui function is associated with the most reactive site [34]. They found that a site having a larger f_k^- value is a better electron donor; whereas one having a larger f_k^+ value is a better electron acceptor. The Fukui function $f(r)$ is defined either as the first derivative of the chemical potential with respect to the external potential V(r) at a constant number of electrons *N* or as the first derivative of the electronic density $\rho(r)$ with respect to the number of electrons N at constant external potential V(r):

$$f(r) = \left[\frac{\delta u}{\delta V(r)}\right]_N = \left[\frac{\partial \rho(r)}{\partial N}\right]_V \quad (2)$$

Because $\rho(r)$ as a function of N has slope discontinuities, three reaction indices of governing electrophilic attack, governing nucleophilic attack, and governing radical attack are provided as follows:

$$f^-(r) = \left[\frac{\partial \rho(r)}{\partial N}\right]_V \quad (3)$$

$$f^+(r) = \left[\frac{\partial \rho(r)}{\partial N}\right]_V \quad (4)$$

$$f^0(r) = 1/2[f^+(r) + f^-(r)] \quad (5)$$

Yang and Mortier [35] defined $f(r)$ in a condensed form; these condensed Fukui functions of an atom k in a molecule with *N* electrons are defined as Eqs. (6), (7), and (8):

$$f_k^+ = [q_k(N+1) - q_k(N)] \quad (6)$$

$$f_k^- = [q_k(N) - q_k(N-1)] \quad (7)$$

$$f_k^0 = 1/2[q_k(N+1) - q_k(N-1)] \quad (8)$$

in which f_k^+, f_k^-, and f_k^0 represent nucleophilic, electrophilic, and radical attack, respectively; q_k is the electronic population of atom *k* in a molecule. Gázquez *et al.* [36] stated that the largest value of the Fukui function is, in general, associated with the most reactive site. According to the Fukui function analysis, when O_2 and CO are adsorbed on the W metal surface, both molecules are electronic acceptors, indicating

the distribution of f_k^- should be considered. In the current study, the f_k^- values were computed by using the Hirshfeld charge according to Eq. (7). Therefore, the distribution of Fukui function (f_k^-) are shown in Figure 3(a) for determining different adsorption sites for O_2 and O on the W nanowire. In Figure 3(a), the W atoms marked in red have the lager f_k^- values, indicating these sites have the higher activity than those marked in blue. It is clear that the helical structure consists of two W one-atom chains with higher reactivity and the other two with lower reactivity, helically entangling with one another. For convenience to present our DFT results, the top sites with higher activity (larger f_k^- values) are designated as T_H, while those with low activity (smaller f_k^- values) are designated as T_L. In Figure 3(b) and 3(c), the local structures around the T_H and T_L are displayed, and the bond between any two W atoms is shown if the distance between these two W atoms is shorter than 2 times Van der Waals radius of W atom (4.20 Å). In Figure 3(b), one can see the bond lengths between two nearest T_H atoms of the same one-atom chain range from 2.711 Å to 2.832 Å, which are slightly longer than those between T_H and T_L atoms ranging from 2.624 Å to 2.645 Å. In Figure 3(c), the T_L atom is bounded by its six nearest W atoms with similar bond lengths. According to the geometrical information about T_H and T_L atoms displayed in Figure 3(b) and 3(c), three types of adsorption sites were considered including top sites (T_H, T_L), bridge sites (B_{H-H}, B_{H-L1}, B_{H-L2}, B_{L-L}) and hollow sites (H_{HHL}, H_{HLL}).

In our previous study [13], three CO oxidation reactions of $CO + O_2 \rightarrow CO_2 + O$, $CO + O + O \rightarrow CO_2 + O$, and $CO + O \rightarrow CO_2$ were considered in ER reaction mechanisms by the W_{10} nanocluster. The intermediate states including the carbonate (CO_3) and peroxo-type (OOCO) are not found for the LH mechanism, because O_2 is easily decomposed to two O atoms on W_{10}, and CO is easier to react with O_2 rather

than O atom. Therefore, only the ER mechanism on the W(111) surface and W helical nanowire was concerned. The optimized geometries of O_2 and O adsorbed on the W helical nanowire are shown in Figure 4 and the corresponding adsorption energies are listed in Table 3.

For O_2-$T_{\mathbf{H}}$-W_{wire} and O_2-$T_{\mathbf{L}}$-W_{wire}, the O_2 molecule was adsorbed at two different top sites of W helical nanowire. The bond lengths of W-O and O-O for O_2-$T_{\mathbf{H}}$-W_{wire} are 1.852 Å and 1.326 Å (Fig. 4(a)). For O_2-$T_{\mathbf{L}}$-W_{wire}, the bond lengths of W-O and O-O are 1.832 Å and 1.322 Å (Fig. 4(b)), respectively. For O_2-$B_{\mathbf{H\text{-}H}}$-W_{wire}, O_2-$B_{\mathbf{H\text{-}L1}}$-W_{wire} and O_2-$B_{\mathbf{L\text{-}L}}$-W_{wire}, the bond lengths of two W-O bonds and the O-O bond for O_2-$B_{\mathbf{H\text{-}H}}$-W_{wire} are 2.030, 2.078 Å and 1.392 Å (Fig. 4(e)), respectively. For O_2-$B_{\mathbf{H\text{-}L1}}$-W_{wire}, the bond lengths of two W-O bonds and the O-O bond are 2.217, 2.048 and 1.367 Å (Fig. 4(f)), respectively. For O_2-$B_{\mathbf{L\text{-}L}}$-W_{wire}, the bond lengths of two W-O bonds and the O-O bond are 2.034, 2.103 Å and 1.392 Å (Fig. 4(i)), respectively. Furthermore, Because of the restriction of geometric configuration, the O_2 at $B_{\mathbf{H\text{-}L2}}$ is decomposed to two O atoms. For the O_2 adsorption, the larger adsorption energies are represented on T_H and $B_{H\text{-}H}$ sites in Table 3, the energies are -2.000 and -2.268 eV, respectively.

For the O adsorbed on the W helical wire surface, the bond lengths of W-O on O-$T_{\mathbf{H}}$-W_{wire} and O-$T_{\mathbf{L}}$-W_{wire} sites are 1.759 Å and 1.748 Å (Figs. 4(c) and 4(d)). On the bridge sites, the bond lengths of two W-O bonds are 1.957 and 1.992 Å for O-$B_{\mathbf{H\text{-}H}}$-W_{wire} (Fig. 4(g)), 2.009 and 1.970 Å for O-$B_{\mathbf{H\text{-}L1}}$-W_{wire} (Fig. 4(h)), and 1.969 and 1.891 Å for O-$B_{\mathbf{L\text{-}L}}$-W_{wire} (Fig. 4(j)). In addition, the bond length of O_2 on $T_{\mathbf{H}}$ site is longer than that of O_2 on $T_{\mathbf{L}}$ site by 0.03 Å, and the weaker bonding leads more easily broken in the oxidation process. Because the O_2 molecule is easily dissociated to two O atoms on the hollow sites of T_H-T_H-T_L, and T_H-T_L-T_L, the hollow sites are

not considered for adsorption energy calculations. Besides, both bond lengths of O_2 molecule on T_H and T_L sites are longer than the gas-phase oxygen bond, because of the charge transfer from the W helical nanowire to the O_2 molecule. The charge transfer causes the increase of electronic density in the antibonding π_g^* orbit of oxygen for the W and O orbital overlapping, resulting in the increment of the O-O bond length. Moreover, although the O atoms adsorbed on the W helical nanowire have larger absorption energy at the bridge sites, it is not the most favorite site for finding barrier. In addition, it should be mentioned that previous studies [37-40] show that the CO_3 and OOCO may exist on gold (Au) and silver (Ag) catalysts, which would be the important precursor states for CO_2 formation. However, both stable adsorption configurations of CO_3 and OOCO species on the W_{10} and W(111) surfaces are not found in our previous work.

Reaction profile for CO oxidation on the W helical nanowire and W(111) Surfaces

On the basis of adsorption results shown in Table 3, the reaction mechanism for CO oxidation on the W helical nanowire and W(111) surfaces were investigated. To find MEP for CO oxidation on W metal surface, the ER reaction mechanism was considered. For the W(111) surface, the CO+O_2 and CO+O energy profiles of CO oxidation process are shown in Figure 5. The reaction of the pathway **I** can be described as $O_{2(ads)}+CO_{(gas)} \rightarrow O_{(ads)}+CO_{2(gas)}$ as shown in Figure 5(a). In pathway **I**, the O_2 adsorbs at Top (I) site. In Figure 5, the pathway I of the ER mechanism starts from the individual CO and O_2 molecules in the gaseous phase as the reactant W(111)+O_2+CO. In the next step, a CO molecule adsorbs on the O_2 molecule. After the dissociation of the adsorbed O_2, the CO directly reacts with O and the energy barrier is 0.70 eV during the reaction. As previously described, because the O_2

dissociates easily on the W surface, the pathway **I** oxidation reaction is more likely to occur, and thus the small energy barrier was observed in this pathway. In pathway **II**, the other reaction $O_{(ads)}+CO_{(gas)} \rightarrow CO_{2(gas)}$ is shown in Figure 5 (b), the CO adsorbs directly on the O atom, and then CO_2 forms by passing through the energy barrier of 1.314 eV. Comparing with pathway **I**, the barrier of pathway **II** is relatively larger, because the O atom possesses the stronger bonding on the W surface. This result indicates that CO is not easy to react with the single O atom, and needs to pass through the high barrier for forming CO_2 molecule.

A similar ER pathway analysis as those on the W(111) surface was also repeated for the W nanowire surface. The potential energy diagrams of $CO+O_2$ and CO+O reactions on the W nanowire are given in Figures 6 (a)-(c), respectively. The pathway I (Figure 6(a)) is considered via the reaction: $O_{2(ads)} + CO_{(gas)} \rightarrow O_{(ads)} + CO_{2(gas)}$. In this reaction, the end-on adsorption of O_2 on the W nanowire surface is considered as the intermediate wire-O_2+CO_{IM1}. To form the final product, $CO_{2(gas)}$, the $CO_{(gas)}$ directly extracts one O atom of adsorbed $O_{2(ads)}$ with the end-on configuration via the transition state with an energy barrier of 0.468 eV. In addition, the adsorbed O_2 with the side-on configuration is not shown in Figure 6(a) because the O_2 bond is always broken when the gas CO is close to the adsorbed O_2 in our calculations. Another possible pathway for CO_2 oxidation is considered by the attachment of CO to an atomic O on the surface directly. This reaction can be described as pathway II of the ER reaction ($O_{(ads)} + CO_{(gas)} \rightarrow CO_{2(gas)}$), as shown in Figure 6(b). In this reaction mechanism, a pathway where the CO molecule reacts with an O atom at the top site (T_H) was concerned. In Figure 6(b), the calculated reaction barrier is 1.529 eV for the formation of CO_2 because the bonding of O on the W nanowire is too strong to react with CO. This result indicates that a much higher energy is required for the formation of CO_2 for an adsorbed O atom when compared to that of O_2.

According to the results of the former adsorption energy calculations as shown in Table 3, the stable configurations are represented on bridge sites. To confirm the lower barriers obtained on top sites, the $O_{(ads)} + CO_{(gas)} \rightarrow CO_{2(gas)}$ reaction at the $B_{H\text{-}H}$ site was described as pathway **III** in Figure 6(c). The calculated reaction barrier is about 2.176 eV for the CO_2 formation. This result reveals the O atom is very difficult to desorb from the bridge site, indicating the bonding of O on the bridge site is too strong to react with CO. In Figure 7, the diffusion barrier of O from $B_{H\text{-}H}$ site to the T_H site is 0.798 eV, which is significantly smaller than the desorption barrier of pathway **III**. This result shows that the O on the T_H site is more prone to react with CO directly.

According to the adsorption results of O and O_2, the bonding of O on the bridge site is too strong to react with CO. However, the bonding of O is demonstrated to become weaker if the O coverage increasing. Due to dissociation of O_2 molecule to O-O atoms occurs easily on W metals, the gas CO_2 will be easily produced by the ER mechanism at the high O coverage. Consequently, the calculated barriers of W nanowire in pathway **I** is smaller than that on the W(111) surface in the same reaction path. However, the W(111) surface represents the better catalytic ability, although the difference is very slight between two materials in pathway **II**.

Analysis of Charge and Electronic State during CO Oxidation

The analyses of charge and electronic state during CO oxidation were conducted by the local density of state (LDOS) onto the orbitals for the adsorbed constructs of O_2 and CO species, as well as for the *d* orbital of bound W atom of the W nanowire and W(111) surface, which are represented in Figures 8(a)-(d). According to the overlapped regions, the extent of orbital hybridization can be observed. Figure 8(a1) and (b1) show the LDOS before the interactions between O_2, CO, and the W nanowire,

respectively. Furthermore, panel (b1) and (b2) show the O_2 and CO molecules interacting with the W nanowire; panel (c1) and (c2) correspond to the LDOS of transition state; panel (d1) and (d2) are the process during CO_2 forms the adsorption configurations on the W helical nanowire. For Figure 8(b1) and (c1), the O_2 on the W nanowire possesses a part of overlap between the $2\pi^*$ orbital of O_2 with the W *d* orbit, indicating the stronger bonding between O_2 and W atom. That is the reason for the O_2 bond length increase while the back-donation from antibonding orbitals $2\pi^*$ of O_2 to W and the electronic resonance between the antibonding orbitals $2\pi^*$ of O_2 and the *d* state of the W atoms. Moreover, it also can be observed the slightly overlaps between the 1π and 5σ orbits of O_2 with the W *d* orbit, and this result explains some electronic transfer from the W atom to O_2. Due to the CO bonds with an adsorbed O_2 by physisorption, there is almost no charge transfer from adsorbed O_2 to CO species. Therefore, the LDOS results do not have remarkable differences in the Figure 8(a2) and (b2). In addition, the LDOS results of transition state show that CO reacts to O_2 nearly in the Figure 8(c2). The orbital hybridization results in the charge transfer, leading to the decrease of the peak of 5σ orbit. Finally, as shown in Figure 8(d2), the LDOS for the products is similar to the separated CO_2 gas phase and adsorbate O on the W nanowire, indicating the CO_2 molecule is only physisorbed on the W nanowire.

Conclusions

The CO oxidation process on the W nanowire has been investigated by the DFT calculation. In the CO oxidation pathways, $CO + O_2 \rightarrow CO_2 + O$, and $CO + O \rightarrow CO_2$ were considered as initial configurations. From the results of adsorption calculations, the O_2 end-on adsorption on a top site is the most stable configuration, while the O atom prefers to adsorb on the bridge site. The corresponding adsorption energies are about -2.0 eV and -4.49 eV, respectively. For the W nanowire and the

W(111) surface, the barriers of pathway **I** about 0.70 eV and 0.468 eV are lower than those of pathway **II** about 1.314 eV and 1.529 eV, respectively. Moreover, the reaction barriers for pathway **I** of the ER mechanism on the W nanowire is smaller than that on the W(111) surface, implying the larger catalytic activity of W nanowire for CO oxidation. According to the back-donation theory from antibonding orbitals $2\pi^*$ of O_2 to W atoms, the bond length changes and adsorption situations have been understood in detail. We hope these DFT simulation results could supply the predictions of structural and electronic properties as well as the perspective viewpoints for the related experiments.

Acknowledgment

The authors would like to thank the funding from the Ministry of Science and Technology under the contract number MOST101-2221-E-110-100-MY3, and are also grateful for the computational time, resources, and facilities from the National Center for High-Performance Computing, Taiwan, and the support from the National Center for Theoretical Sciences, Taiwan.

Reference

[1] H.-T. Chen, D. G. Musaev, and M. C. Lin, "Adsorption and Dissociation of COx (x = 1, 2) on W(111) Surface : A Computational Study," *The Journal of Physical Chemistry C,* vol. 112, pp. 3341-3348, 2008/03/01 2008.

[2] S.-F. Peng and J.-J. Ho, "Theoretical Study of H2S Dissociation and Sulfur Oxidation on a W(111) Surface," *The Journal of Physical Chemistry C,* vol. 114, pp. 19489-19495, 2010/11/18 2010.

[3] H.-T. Chen, H.-L. Chen, S.-P. Ju, D. G. Musaev, and M. C. Lin, "Density Functional Studies of the Adsorption and Dissociation of NOx (x = 1, 2) Molecules on the W(111) Surface," *The Journal of Physical Chemistry C,* vol. 113, pp. 5300-5307, 2009/04/02 2009.

[4] R. B. Levy and M. Boudart, "Platinum-Like Behavior of Tungsten Carbide in Surface Catalysis," *Science,* vol. 181, pp. 547-549, August 10, 1973 1973.

[5] K. E. Johnson, R. J. Wilson, and S. Chiang, "Effects of adsorption site and surface stress on ordered structures of oxygen adsorbed on W(110)," *Physical Review Letters,* vol. 71, pp. 1055-1058, 08/16/ 1993.

[6] J. C. Buchholz and M. G. Lagally, "Order-Disorder Transition and Adatom-Adatom Interactions in a Chemisorbed Overlayer: Oxygen on W(110)," *Physical Review Letters,* vol. 35, pp. 442-445, 08/18/ 1975.

[7] M. A. Van Hove and S. Y. Tong, "Chemisorption Bond Length and Binding Location of Oxygen in a p(2×1) Overlayer on W(110) Using a Convergent, Perturbative, Low-Energy-Electron-Diffraction Calculation, " *Physical Review Letters,* vol. 35, pp. 1092-1095, 10/20/ 1975.

[8] T.-U. N. a. R. Gomer, "The diffusion of oxygen on W(110) revisited " *J. Chem. Phys.,* vol. 106, p. 10349, 1997.

[9] E. A. Daniels and R. Gomer, "The diffusion of oxygen on W(001)," *Surface Science,* vol. 397, pp. 209-216, 2/1/ 1998.

[10] M. T. a. R. Gomer, "Diffusion anisotropy of oxygen and of tungsten on the tungsten (211) plane," *J. Chem. Phys.,* vol. 84, p. 13 pages, 1986.

[11] M. H. Weng, J. Y. Hsieh, S. P. Ju, J. G. Chang, H. T. Chen, H. L. Chen*, et al.*, "Adsorption and Dissociation of the O2 on W(111) Surface: A Density Functional Theory Study," *Journal of Nanoscience and Nanotechnology,* vol. 10, pp. 7196-7199, // 2010.

[12] L. Chen, D. S. Sholl, and J. K. Johnson, "First Principles Study of Adsorption and Dissociation of CO on W(111)," *The Journal of Physical Chemistry B,* vol. 110, pp. 1344-1349, 2006/01/01 2005.

[13] M. H. Weng and S. P. Ju, "CO Oxidation Mechanism on Tungsten Nanoparticle," *The Journal of Physical Chemistry C,* vol. 116, pp.

18803-18815, 2012/09/06 2012.

[14] C. T. Campbell, S. C. Parker, and D. E. Starr, "The Effect of Size-Dependent Nanoparticle Energetics on Catalyst Sintering," *Science,* vol. 298, pp. 811-814, October 25, 2002 2002.

[15] G. Kresse and J. Hafner, "Ab initio molecular dynamics for liquid metals," *Physical Review B,* vol. 47, pp. 558-561, 01/01/ 1993.

[16] W. An, Y. Pei, and X. C. Zeng, "CO Oxidation Catalyzed by Single-Walled Helical Gold Nanotube," *Nano Letters,* vol. 8, pp. 195-202, 2008/01/01 2007.

[17] G. Kresse and J. Hafner, "Ab initio molecular dynamics for liquid metals," *Physical Review B,* vol. 47, pp. 558-561, 01/01/ 1993.

[18] B. Hammer, L. B. Hansen, and J. K. Nørskov, "Improved adsorption energetics within density-functional theory using revised Perdew-Burke-Ernzerhof functionals," *Physical Review B,* vol. 59, pp. 7413-7421, 03/15/ 1999.

[19] M. Iwamatsu and Y. Okabe, "Basin hopping with occasional jumping," *Chemical Physics Letters,* vol. 399, pp. 396-400, 2004.

[20] V. Rosato, M. Guillope, and B. Legrand, "Thermodynamical and Structural-Properties of Fcc Transition-Metals Using a Simple Tight-Binding Model," *Philosophical Magazine a-Physics of Condensed Matter Structure Defects and Mechanical Properties,* vol. 59, pp. 321-336, Feb 1989.

[21] S.-J. Sun, K.-H. Lin, S.-P. Ju, and J.-Y. Li, "Electronic and structural properties of ultrathin tungsten nanowires and nanotubes by density functional theory calculation," *Journal of Applied Physics,* vol. 116, pp. -, 2014.

[22] L. Hui, B. L. Wang, J. L. Wang, and G. H. Wang, "Local atomic structures of palladium nanowire," *The Journal of Chemical Physics,* vol. 121, pp. 8990-8996, 2004.

[23] A. Ulitsky and R. Elber, "A new technique to calculate steepest descent paths in flexible polyatomic systems," *The Journal of Chemical Physics,* vol. 92, pp. 1510-1511, 1990.

[24] G. Mills, H. Jónsson, and G. K. Schenter, "Reversible work transition state theory: application to dissociative adsorption of hydrogen," *Surface Science,* vol. 324, pp. 305-337, 2/10/ 1995.

[25] H. J. F. Jansen and A. J. Freeman, "Total-energy full-potential linearized augmented-plane-wave method for bulk solids: Electronic and structural properties of tungsten," *Physical Review B,* vol. 30, pp. 561-569, 07/15/ 1984.

[26] J. Du, X. Sun, D. Meng, P. Zhang, and G. Jiang, "Geometrical and electronic structures of small Wn(n=2–16) clusters," *The Journal of Chemical Physics,* vol. 131, p. 044313, 2009.

[27] M. J. Mehl and D. A. Papaconstantopoulos, "Applications of a tight-binding total-energy method for transition and noble metals: Elastic constants, vacancies, and surfaces of monatomic metals," *Physical Review B,* vol. 54, pp. 4519-4530, 08/15/ 1996.

[28] Z. Hu, J. G. Dong, J. R. Lombardi, and D. M. Lindsay, "Optical and Raman spectroscopy of mass-selected tungsten dimers in argon matrices," *The Journal of Chemical Physics,* vol. 97, pp. 8811-8812, 1992.

[29] M. D. Morse, "Clusters of transition-metal atoms," *Chemical Reviews,* vol. 86, pp. 1049-1109, 1986/12/01 1986.

[30] B. G. Johnson, P. M. W. Gill, and J. A. Pople, "The performance of a family of density functional methods," *The Journal of Chemical Physics,* vol. 98, pp. 5612-5626, 1993.

[31] S. Chrétien, S. K. Buratto, and H. Metiu, "Catalysis by very small Au clusters," *Current Opinion in Solid State and Materials Science,* vol. 11, pp. 62-75, 10// 2007.

[32] K. Fukui, "Role of Frontier Orbitals in Chemical Reactions," *Science,* vol. 218, pp. 747-754, November 19, 1982 1982.

[33] L. M. Falicov and G. A. Somorjai, "Correlation between catalytic activity and bonding and coordination number of atoms and molecules on transition metal surfaces: Theory and experimental evidence," *Proceedings of the National Academy of Sciences of the United States of America,* vol. 82, pp. 2207-2211, 1985.

[34] R. G. Parr and W. Yang, "Density functional approach to the frontier-electron theory of chemical reactivity," *Journal of the American Chemical Society,* vol. 106, pp. 4049-4050, 1984/07/01 1984.

[35] W. Yang and W. J. Mortier, "The use of global and local molecular parameters for the analysis of the gas-phase basicity of amines," *Journal of the American Chemical Society,* vol. 108, pp. 5708-5711, 1986/09/01 1986.

[36] J. L. Gazquez and F. Mendez, "The Hard and Soft Acids and Bases Principle: An Atoms in Molecules Viewpoint," *The Journal of Physical Chemistry,* vol. 98, pp. 4591-4593, 1994/04/01 1994.

[37] H.-T. Chen, J.-G. Chang, S.-P. Ju, and H.-L. Chen, "First-principle calculations on CO oxidation catalyzed by a gold nanoparticle," *Journal of Computational Chemistry,* vol. 31, pp. 258-265, 2010.

[38] Z.-P. Liu, P. Hu, and A. Alavi, "Catalytic Role of Gold in Gold-Based Catalysts: A Density Functional Theory Study on the CO Oxidation on Gold," *Journal of the American Chemical Society,* vol. 124, pp. 14770-14779, 2002/12/01 2002.

[39] H. Y. Kim, S. S. Han, J. H. Ryu, and H. M. Lee, "Balance in Adsorption Energy of Reactants Steers CO Oxidation Mechanism of Ag13 and Ag12Pd1 Nanoparticles: Association Mechanism versus Carbonate-Mediated Mechanism," *The Journal of Physical Chemistry C,* vol. 114, pp. 3156-3160, 2010/02/25 2010.

[40] H.-Y. Su, M.-M. Yang, X.-H. Bao, and W.-X. Li, "The Effect of Water on the CO Oxidation on Ag(111) and Au(111) Surfaces: A First-Principle Study," *The Journal of Physical Chemistry C,* vol. 112, pp. 17303-17310, 2008/11/06 2008.

[41] Graeme Henkelman, and Hannes Jo´nsson, " Improved tangent estimate in the nudged elastic band method for finding minimum energy paths and saddle points", *The Journal of Chemical Physics,* vol. 113, pp 9978-9985

Table 1 The results of binding energy using rPBE functional for bulk tungsten materials

		Exp.	***DFT***
$\mathbf{W_{FCC}}$	Cohesive Energy (eV)	8.33~8.45[a]	8.61
$\mathbf{W_{HCP}}$		8.33[b]	8.19
$\mathbf{W_{BCC}}$		8.9[a]	8.94
	Lattice constant (Å)	3.16[b] 3.25[c]	3.16

[a]Reference [25], [b]Reference [26], [c]Reference[27], [d]Reference [32]

Table 2 The results of bonding, frequency, and dissociative energy using rPBE functional for the tungsten dimer

	Method	**R (Å)**	**ω(cm^{-1})**	**E_d(eV)**
W_2	rPBE/DNP/DSPP	2.075[g]	334.2[g]	4.74[g]
	Exp.		337[e]	5 ±1[f]

[e]Reference [28], [f]Reference [29], [g]This work

Table 3 The adsorption energy and bond lengths of O atom and O_2 molecule on the W helical nanowire.

Species	**Bond length(Å) (O-O)**	**Bond length(Å) (W-O)**	**Adsorption energy(eV)**
O_2 molecule			
T_H	1.326	1.852	-2.000
T_L	1.322	1.832	-1.980
B_{H-H}	1.372	2.034, 1.958	-2.268
B_{H-L1}	1.370	2.197, 2.056	-1.219
B_{L-L}	1.392	2.041, 2.103	-1.793
O atom			
T_H		1.759	-3.853
T_L		1.748	-3.888
B_{H-H}		1.957, 1.992	-4.490
B_{H-L1}		2.009, 1.970	-3.194
B_{L-L}		1.969,1.891	-3.974

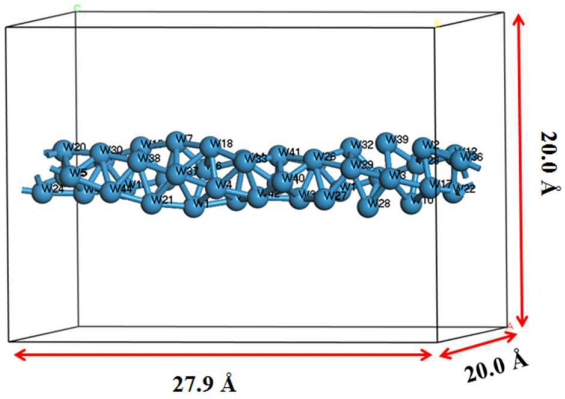

(a)

Figure 1 (a) Optimized geometry of the W helical nanowire

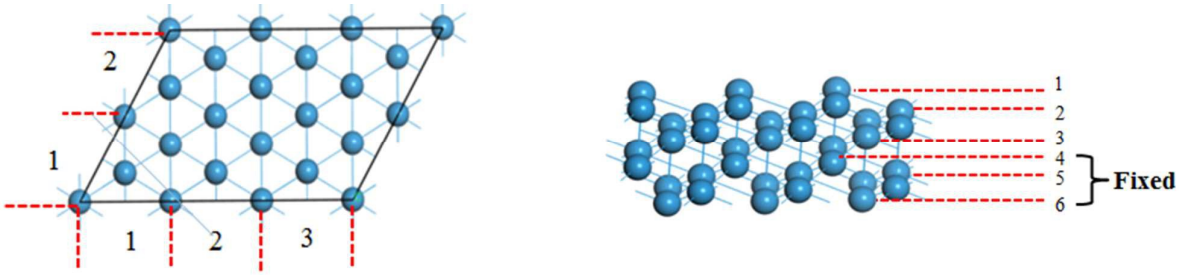

Figure 2 schematic diagram of *p*(3×2) W(111) surface: (left) top view; (right) side view.

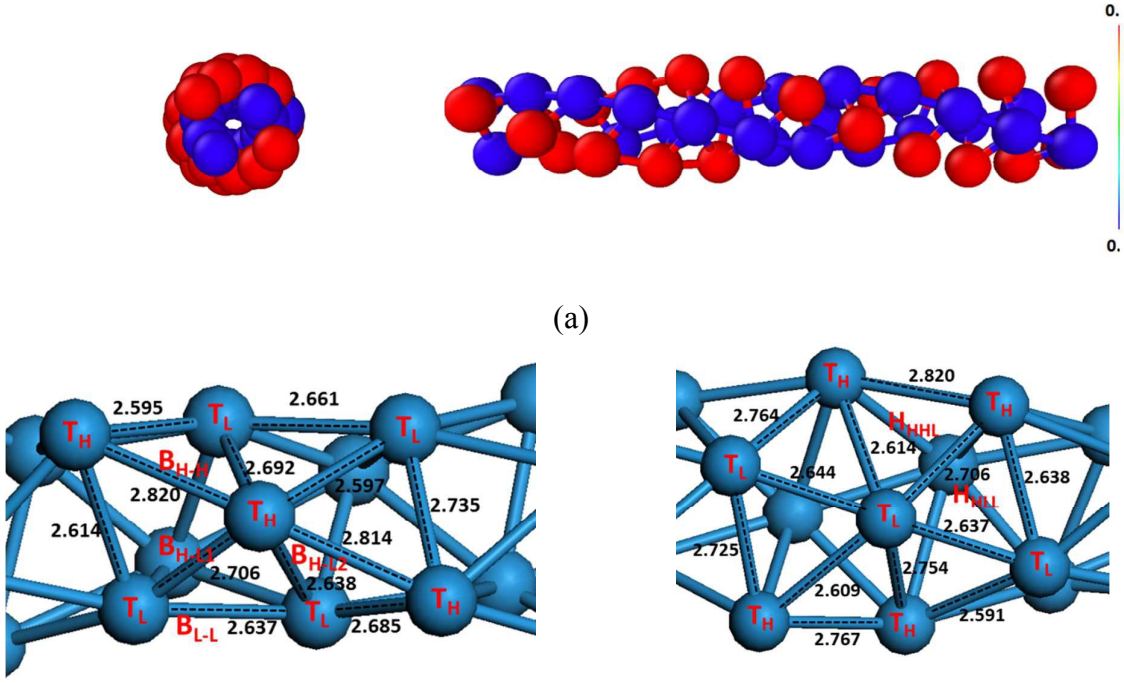

Figure 3 Fukui function F^{k-} of the W helical nanowire: (left) cross-section view; (right) side view (b) The bond length of the high activity region. (c) The bond length of the low activity region. The labels T, B and H represent top, bridge, and hollow sites. The subscript of the labels H, L represent high and low activity region. Note that the bridge sites are between every two surface W atoms, and the hollow sites are in the middle sites of three W atoms.

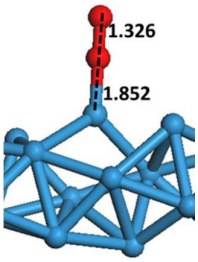

(a) O_2 On-Top (T_H)

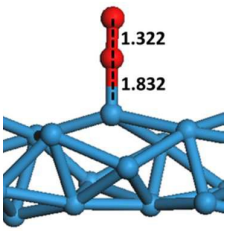

(b) O_2 On-Top (T_L)

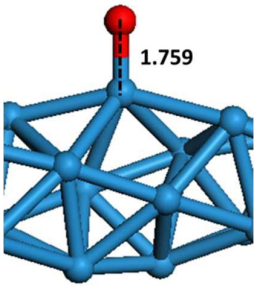

(c) O On-Top (T_H)

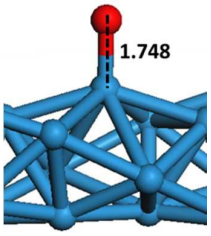

(d) O On-Top (T_L)

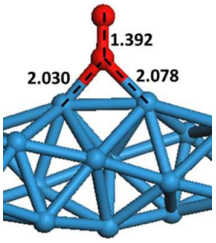

(e) O_2 Bridge **(H-H)**

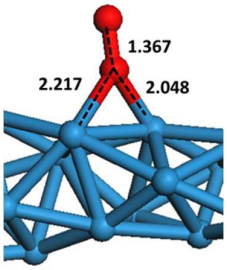

(f) O_2 Bridge **(H-L1)**

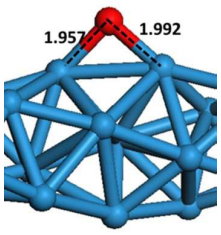

(g) O Bridge (**H-H**)

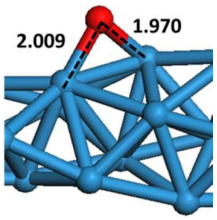

(h) O Bridge (**H-L1**)

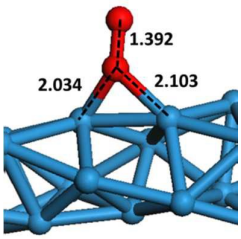

(i) O_2 Bridge (**L-L)**

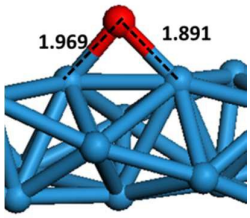

(j) O Bridge (**L-L)**

Figure 4 Optimized geometries of O_2 and O adsorption on the W nanowire. The bond lengths are given in angstroms (Å).

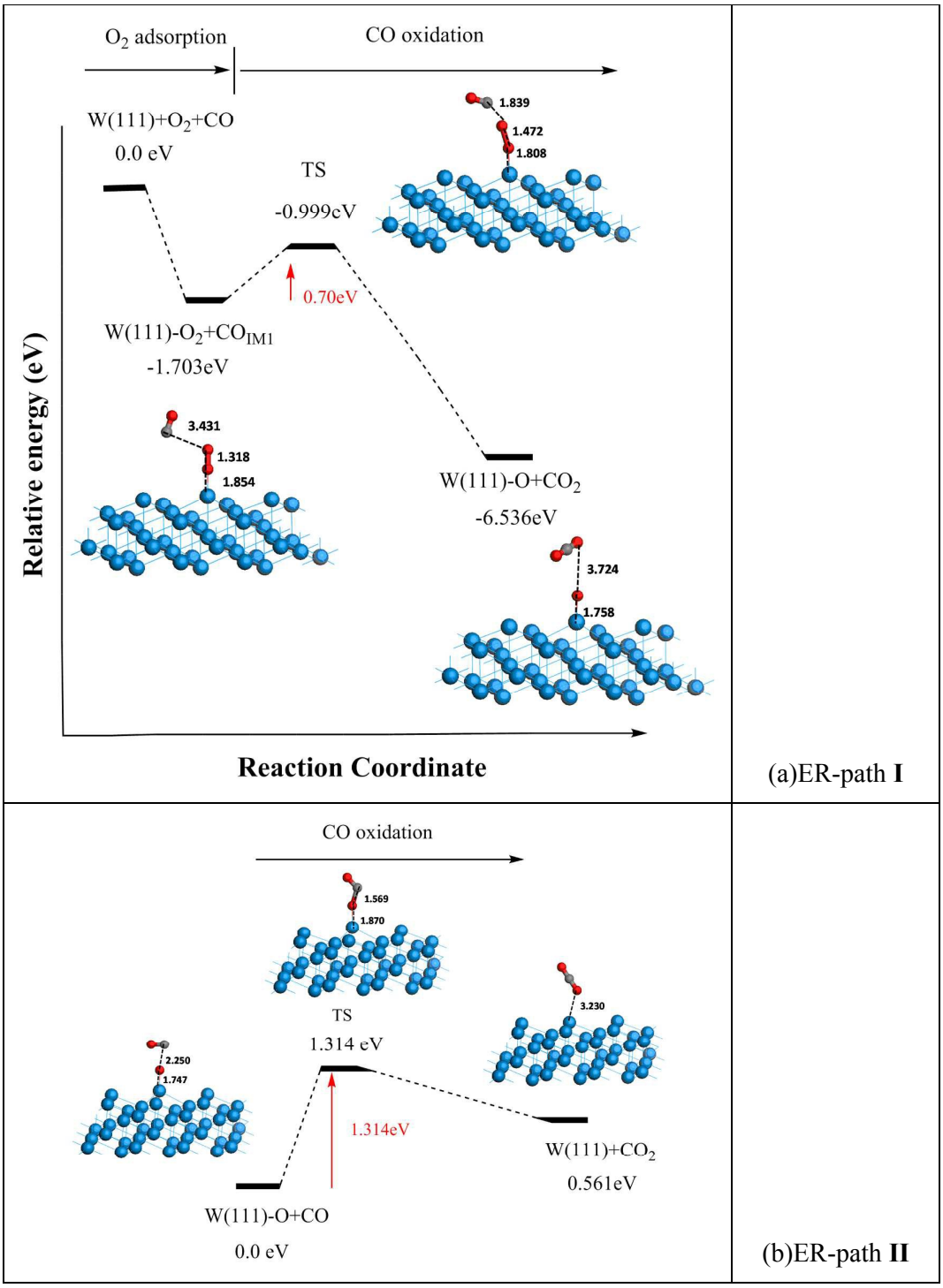

Figure 5 Schematic potential energy profiles of the ER reaction paths for (a) CO + O_2 and (b) CO + O reactions on the W(111) surface.

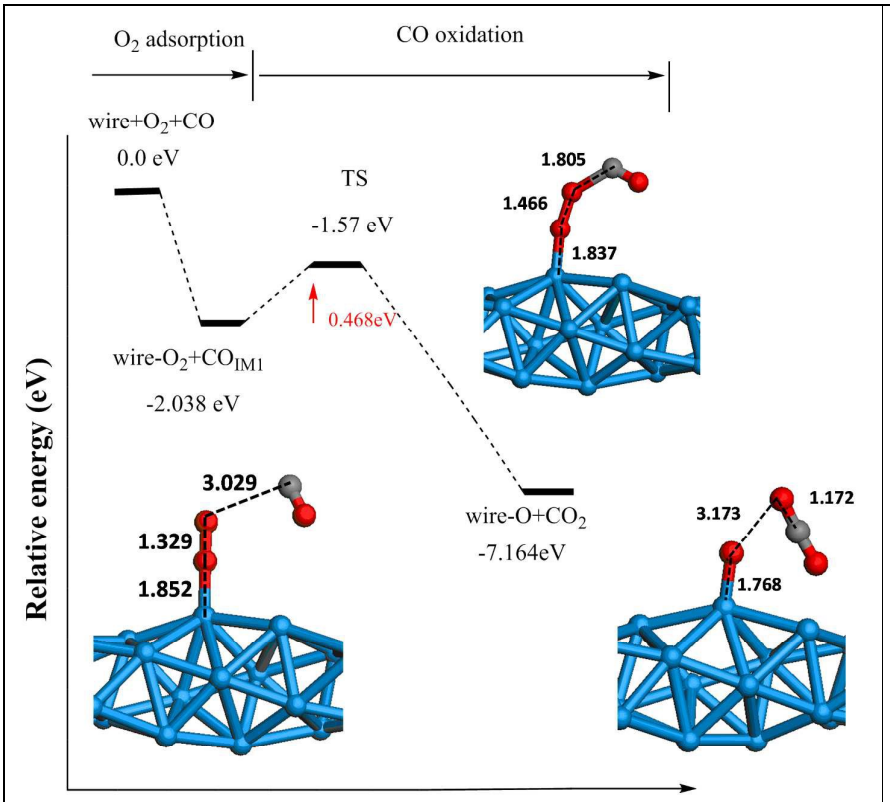

(a)ER-path **I**

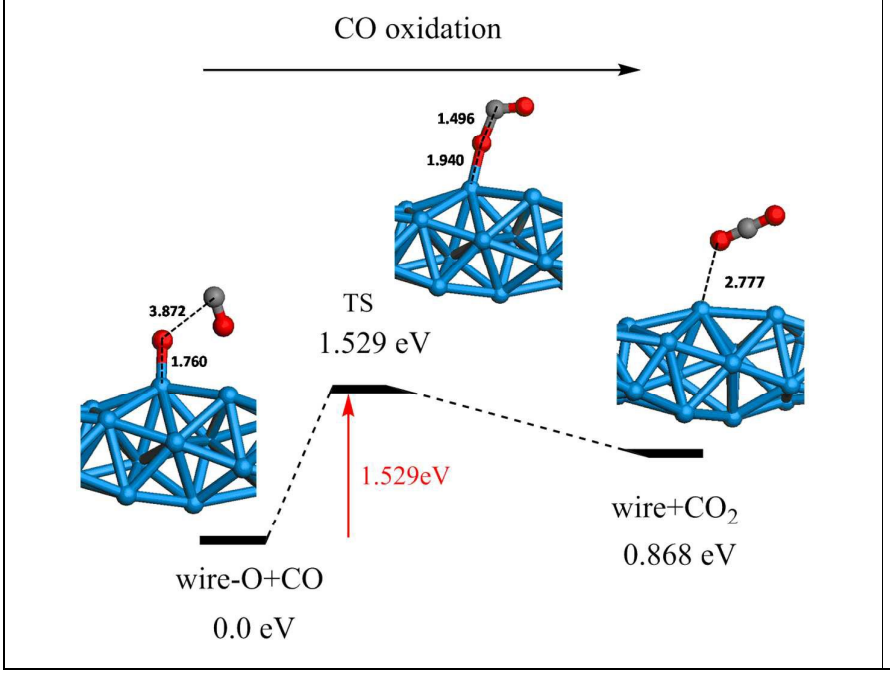

(b)ER-path **II**

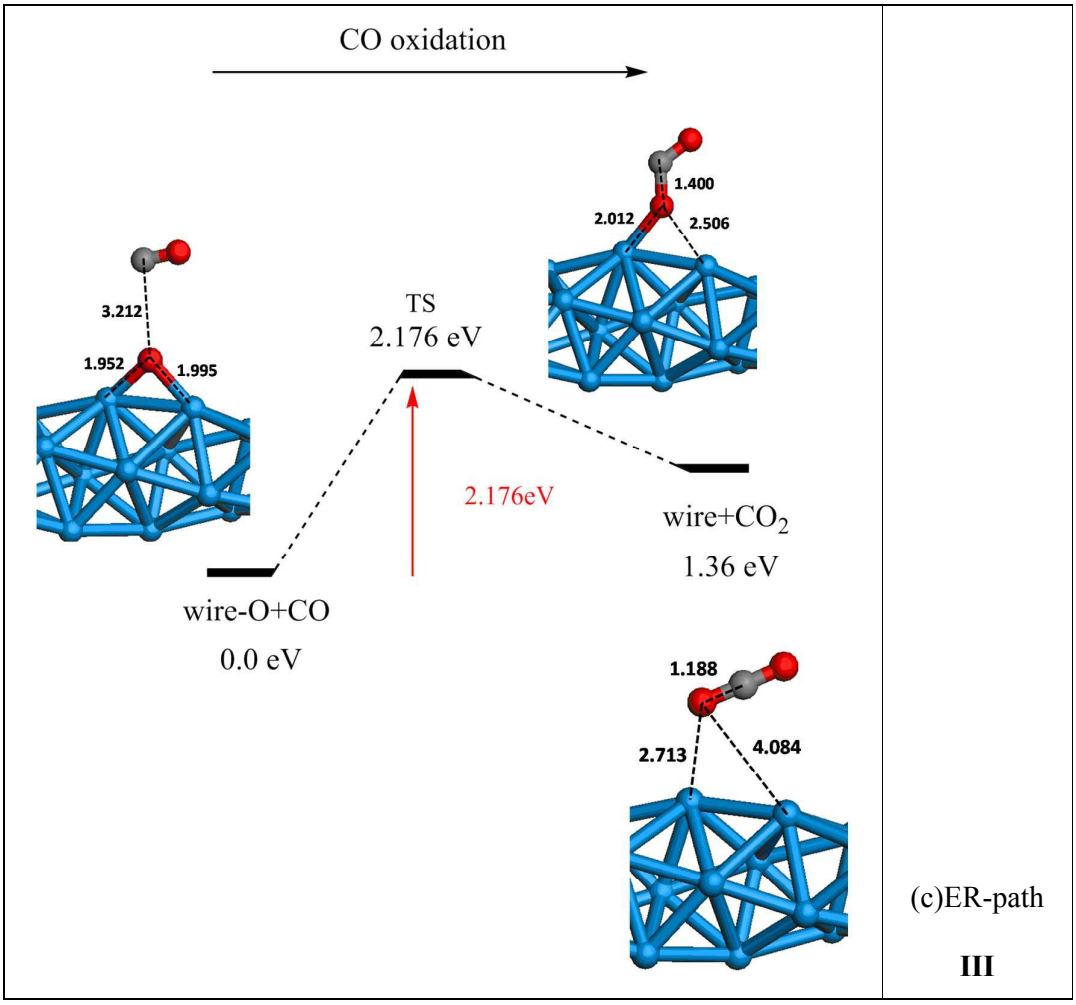

Figure 6 Schematic potential energy profiles of the ER reaction path for (a) CO + O_2, (b) CO + O(on top site), and (c) CO + O (on bridge site) reactions on the W nanowire.

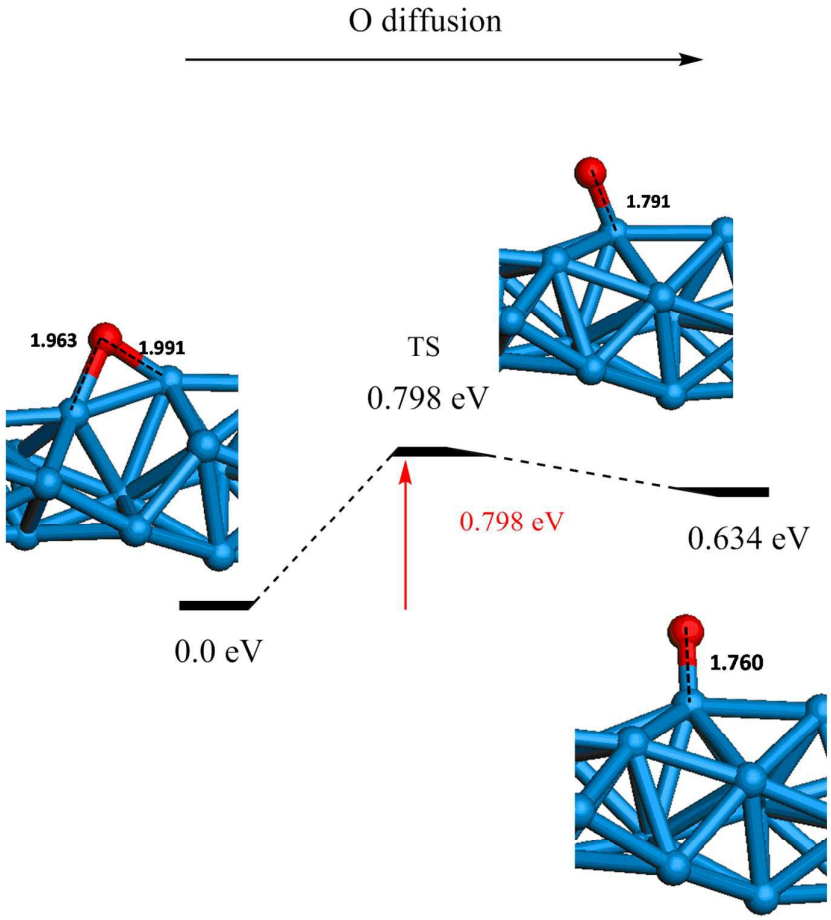

Figure 7 Schematic potential energy profiles of the diffusion reaction from $B_{H\text{-}H}$ site to the T_H site on the W nanowire.

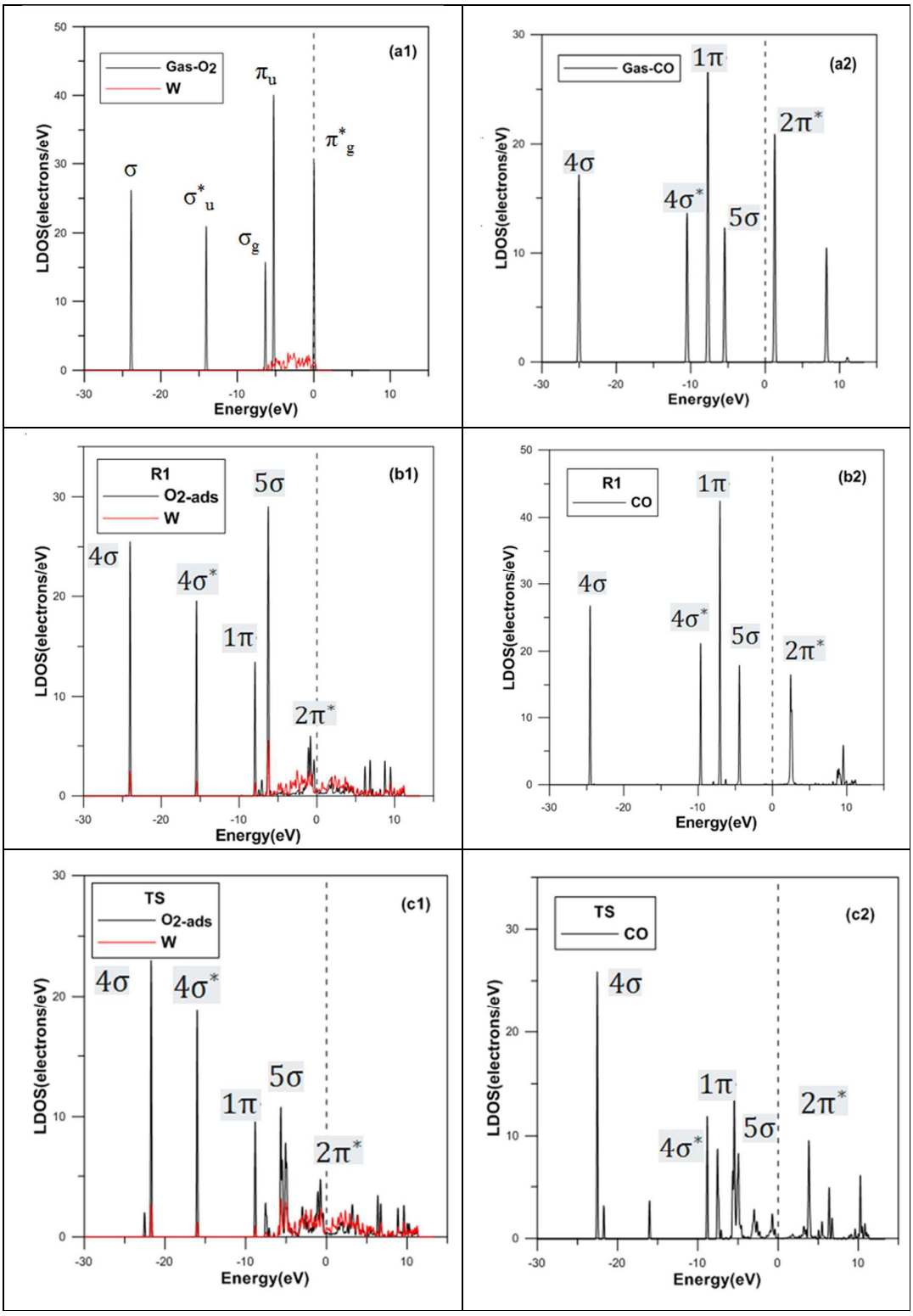

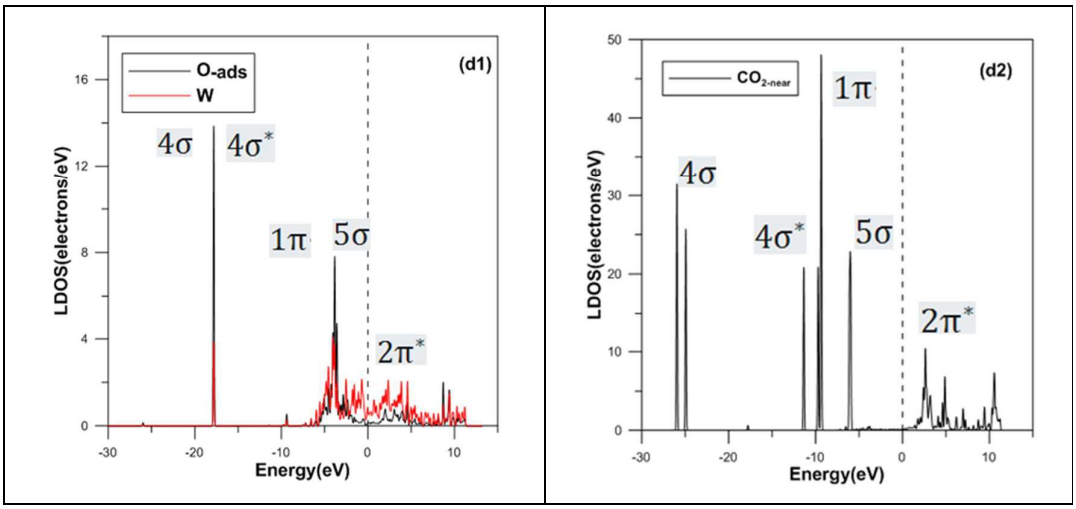

Figure 8 Partial density of states (PDOS) projected onto O−O and C−O for CO oxidation on the W helical nanowire: (a) before interaction; (b) W_{wire}−O_2 and CO molecule interacting with the W_{wire}; (c) transition state; (d) W_{wire}−O and CO_2 molecule interacting with the W_{wire}. The dashed line represents the Fermi level.